MID-AMERICA TRANSPORTATION CENTER

Final Report
WBS: 25-1121-3002-101
Report # MATC: 101

Improving Safety by Eliminating the Bump at End of the Bridge Using Lightweight Backfill and Geosynthetics

Jie Han, Ph.D., P.E., F.ASCE
Roy A. Roberts Distinguished Professor
Department of Civil, Environmental, and Architectural Engineering
The University of Kansas

Hao Liu, Ph.D.
Associate Professor
School of Civil Engineering
Chongqing Jiaotong University

Yuqiu Ye, Ph.D.
Research Associate
Department of Civil, Environmental, and Architectural Engineering
The University of Kansas

Robert L. Parsons, Ph.D., P.E. F.ASCE
Professor
Department of Civil, Environmental, and Architectural Engineering
The University of Kansas

2025

A Cooperative Research Project sponsored by the U.S. Department of Transportation-Office of the Assistant Secretary for Research and Technology.

Improving Safety by Eliminating the Bump at End of the Bridge Using Lightweight Backfill and Geosynthetics

Jie Han, Ph.D., P.E., F.ASCE
Roy A. Roberts Distinguished Professor
Department of Civil, Environmental, and Architectural Engineering
The University of Kansas

Yuqiu Ye, Ph.D.
Research Associate
Department of Civil, Environmental, and Architectural Engineering
The University of Kansas

Hao Liu, Ph.D.
Associate Professor
School of Civil Engineering
Chongqing Jiaotong University

Robert L. Parsons, Ph.D., P.E., F.ASCE
Professor
Department of Civil, Environmental, and Architectural Engineering
The University of Kansas

A Report on Research Sponsored by

Mid-America Transportation Center
University of Nebraska–Lincoln

June 2025

Technical Report Documentation Page

1. Report No. 25-1121-3002-101	2. Government Accession No.	3. Recipient's Catalog No.
4. Title and Subtitle Improving Safety by Eliminating the Bump at End of the Bridge Using Lightweight Backfill and Geosynthetics		5. Report Date June 2025
		6. Performing Organization Code
7. Author(s) Jie Han ORCID No. 0000-0003-3137-733X Yuqiu Ye ORCID No. 0009-0004-7216-5725 Hao Liu ORCID No. 0000-0002-5906-4899, and Robert L. Parsons ORCID No. 0000-0002-9030-5777		8. Performing Organization Report No. 25-1121-3002-101
9. Performing Organization Name and Address Mid-America Transportation Center Prem S. Paul Research Center at Whittier School 2200 Vine St. Lincoln, NE 68583-0851		10. Work Unit No. (TRAIS)
		11. Contract or Grant No. 69A3552348307
12. Sponsoring Agency Name and Address Office of the Assistant Secretary for Research and Technology 1200 New Jersey Ave., SE Washington, D.C. 20590		13. Type of Report and Period Covered 06/01/2023 - 05/30/2025
		14. Sponsoring Agency Code
15. Supplementary Notes		

16. Abstract
Seasonal temperature changes induce the expansion and contraction of bridge girders and decks which move integral bridge abutments (IBAs) toward and away from their backfill, resulting in high horizontal earth pressures, backfill surface settlements, and abutment toe movements away from the backfill. Geosynthetic reinforcements can provide tensile resistance and have good interactions with soil, while lightweight aggregate has low self-weight and a high friction angle. These characteristics may enable geosynthetic reinforcement and lightweight aggregate to mitigate the seasonal temperature change-induced problems associated with the IBAs. This study utilized finite difference method-based software FLAC2D to assess the benefits of geosynthetic reinforcement and lightweight aggregate in addressing the seasonal temperature change-induced problems with IBAs. The plastic hardening soil model was used to simulate the behavior of the backfill while the strip elements were used to simulate geosynthetics. Numerical results show that geosynthetic reinforcement connected to the abutment reduced the total and differential settlements behind the abutment and minimized the development of potential shear slip surfaces within the backfill. Lightweight aggregate as an abutment backfill reduced the horizontal earth pressures behind the abutment but might develop multiple active and passive shear slip surfaces after simulated seasonal temperature changes. The combined measures of the lightweight aggregate and the geosynthetic reinforcements connected to the abutment best reduced the total and differential settlements, minimized the development of active and passive shear slip surfaces within the backfill, and reduced the horizontal earth pressures behind the abutment.

17. Key Words Geosynthetic, Lightweight aggregate, Integral bridge abutment, Seasonal temperature change.	18. Distribution Statement		
19. Security Class if. (of this report) Unclassified	20. Security Class if. (of this page) Unclassified	21. No. of Pages 45	22. Price

Table of Contents

List of Tables

List of Figures

Acknowledgments

The U.S. Department of Transportation provided financial support for this research through the University of Nebraska-Lincoln Mid-America Transportation Center under contract number 69A3552348307.

Disclaimer

The contents of this report reflect the views of the authors, who are responsible for the facts and the accuracy of the information presented herein. This document is disseminated in the interest of information exchange. The report is funded by a grant from the U.S. Department of Transportation's University Transportation Centers Program. However, the U.S. Government assumes no liability for the contents or use thereof.

Abstract

Seasonal temperature changes induce the expansion and contraction of bridge girders and decks which move integral bridge abutments (IBAs) toward and away from their backfill, resulting in high horizontal earth pressures, backfill surface settlements, and abutment toe movements away from the backfill. Geosynthetic reinforcements can provide tensile resistance and have good interactions with soil, while lightweight aggregate has low self-weight and a high friction angle. These characteristics may enable geosynthetic reinforcement and lightweight aggregate to mitigate the seasonal temperature change-induced problems associated with the IBAs. This study utilized finite difference method-based software FLAC2D to assess the benefits of geosynthetic reinforcement and lightweight aggregate in addressing the seasonal temperature change-induced problems with IBAs. The plastic hardening soil model was used to simulate the behavior of the backfill while the strip elements were used to simulate geosynthetics.

Numerical results show that geosynthetic reinforcement connected to the abutment reduced the total and differential settlements behind the abutment and minimized the development of potential shear slip surfaces within the backfill. Lightweight aggregate as an abutment backfill reduced the horizontal earth pressures behind the abutment but might develop multiple active and passive shear slip surfaces after simulated seasonal temperature changes. The combined measures of the lightweight aggregate and the geosynthetic reinforcements connected to the abutment best reduced the total and differential settlements, minimized the development of active and passive shear slip surfaces within the backfill, and reduced the horizontal earth pressures behind the abutment.

Chapter 1 Introduction

1.1 Background and Problem Statement

Bridges are important infrastructure components that facilitate transportation and connectivity. However, their structural integrity is influenced by various factors, including seasonal temperature changes. The expansion and contraction of bridge components due to temperature changes significantly affect the performance of bridge abutments, which serve as the structural supports at both ends of a bridge. The bridge abutment movements induce horizontal earth pressures and differential settlements, i.e., bumps. The bump at the end of the bridge is a universal problem for bridges around the world including the US. This problem has caused many motor vehicle fatalities and requires more than 100 million dollars annually to maintain and repair in the US alone.

Lightweight backfill has low self-weight while geosynthetics—factory-manufactured polymer sheets—have high tensile strengths. The proper selection of lightweight bridge abutment backfill materials reinforced by geosynthetics may significantly reduce horizontal earth pressures and backfill surface settlements, thus eliminating or minimizing bumps at the end of bridges. A laboratory study done by this research team using sands as backfill materials reinforced by geosynthetics has demonstrated the effectiveness of the technology. This research is to improve the previous technology by replacing sands with lightweight aggregates. This innovative technology requires a numerical study verification.

1.2 Objectives

The main objective of this research is to verify the effectiveness of using lightweight aggregates reinforced by geosynthetics for bridge abutments to eliminate or minimize bumps at the end of bridges and improve the safety of highways and railways. This technology will have

broader impacts on the safety of bridge approaches and the economy of bridge maintenance and repair.

1.3 Research Methodology

This study adopted the following research methodology:

(1) Conduct a literature review to summarize the state of the knowledge in integral bridge abutments and seasonal temperature change-induced integral bridge abutment issues (e.g., horizontal earth pressures and settlements) and

(2) Conduct numerical simulations to evaluate the performance of lightweight aggregates and geosynthetic reinforcement to mitigate the seasonal temperature change-induced integral bridge abutment issues.

1.4 Report Organization

This report consists of five chapters. Chapter one presents an introduction including background and problem statements, objective, research methodology, and organization of the report. Chapter two presents the literature review on seasonal temperature change-induced integral bridge abutment issues (e.g., horizontal earth pressures and settlements). Chapter three presents the numerical model calibration, material properties, and simulation arrangement. Chapter four presents numerical simulation results to evaluate the performance of lightweight aggregate and geosynthetic reinforcement to mitigate the seasonal temperature change-induced integral bridge abutment issues. Chapter five provides the conclusions.

Chapter 2 Literature Review

Integral Bridge Abutments (IBAs) or Integral Abutment Bridges (IABs) are one type of bridge system that has continuous and monolithic decks supported by two ends of abutments without any expansion joints. Burke (1993), Tatsuoka et al. (2009), Liu et al. (2022a), Abdullah and El Naggar (2023), and Liu et al. (2025) summarized several advantages of IABs over conventional bridges, including but not limited to: (1) reduced overall cost through the elimination of costly materials as well as installation and maintenance of expansion bearings and joints; (2) improved ride quality by removing expansion joints (often the source of discomfort and maintenance issues); (3) faster and more economical construction due to fewer piles required for abutment support; (4) simplified structural design by integrating the superstructure, abutments, and piles into a continuous frame system; (5) enhanced seismic performance as a result of rigid connections between the superstructure and abutments (improving structural integrity during earthquakes); and (6) reduced buoyancy forces during extreme events such as hurricanes and tsunamis, owing to thinner superstructure. As a result, IBAs have been increasingly used by different state departments of transportation in the United States over the past 30 years.

However, IBAs are more sensitive to seasonal/temperature changes due to end constraints; therefore, they have been increasingly studied through experimental tests and numerical simulations. Liu et al (2022b) conducted model tests to study the settlement and horizontal earth pressure behind the IBA induced by simulated seasonal temperature changes and revealed that the backfill surface settlement near the abutment depended on the abutment footing rigidity and the magnitude of abutment movement and its variation continued even after 30 cycles of abutment movement. Liu et al. (2025) evaluated the structural behavior of IBA approach slabs subjected to live loads and thermal effects and found that when an approach slab was subjected to the combined effects of low temperature and solar radiation, its principal stress could reach the modulus of

rupture. Alqarawi et al. (2016) found that the abutment cyclic movement resulted in the settlement of the approach soil and increased horizontal earth pressures on the abutment wall. In their model tests, Zadehmohamad and Bazaz (2017) found that geocell reinforcement significantly reduced the coefficient of peak horizontal earth pressure behind the abutment wall subjected to cyclic loading. Through numerical simulations of IABs with composite steel I-girders subjected to seasonal temperature changes, LaFave et al. (2016) found that the effective expansion length of the girders had a primary influence on bridge longitudinal movement under thermal loads.

To mitigate the temperature change-induced problems for IBAs, rubberized soils, geocell-reinforced backfill, geogrid-reinforced backfill, waste tire bales (compressed and compacted packages of used tires), or expanded polystyrene (EPS) blocks have been used to replace typical aggregate backfill, reduce horizontal earth pressures behind the abutment as the abutment moves toward the backfill, and reduce seasonal temperature change-induced backfill surface settlements (Cui and Mitoulis, 2015; Zadehmohamad and Bazaz, 2017; Duda and Siwowski, 2020; Farhangi et al. 2023). In addition, a compressible inclusion (e.g., EPS foam, tire shred, or tire-derived aggregates) has been placed between the abutment and the backfill to reduce the horizontal earth pressures behind the abutment and the pile moment (Hoppe, 2005; Caristo et al., 2018; Duda and Siwowski, 2020; Liu et al., 2021; Zadehmohamad et al., 2021). Lightweight aggregate (e.g., expanded shale, clay, and slate) has lower self-weight and a higher friction angle compared to typical soil and has been increasingly used as a backfill material for embankments, retaining walls, and pipelines (Liu et al. 2022c; Ye et al. 2022, 2024). Geosynthetic reinforcement can provide tensile strength and has good interaction with soil. Intuitively, the combined use of lightweight aggregate (LWA) with geosynthetic reinforcement as an IBA backfill material may mitigate seasonal temperature change-induced problems; however, such an application has not been studied.

To better understand the performance of geosynthetic reinforcement and lightweight aggregate to mitigate the seasonal temperature change-induced problems for IBAs, this study carried out two-dimensional (2D) numerical analyses. The numerical results will be used to assess the mitigation effects of geosynthetic reinforcement and lightweight aggregate on the abutment toe movements, backfill surface settlements, and horizontal earth pressures.

Chapter 3 Numerical Simulation Setup

3.1 Numerical model

Figure 3.1 shows the numerical model for the case without any mitigation measures as the baseline model. This model was developed to simulate a physical model test in the publication by Liu et al. (2022b). In the physical model test, the test box was constructed using wooden panels reinforced with steel tube beams and rested on the ground. Accordingly, the base of the numerical model had a two-layer system, consisting of a 0.20-m thick concrete layer beneath a 0.15-m thick wooden layer. Additionally, a 0.05-m thick wooden plate was included on the right side to simulate the support for the backfill in the physical model. The backfill was 1.46 m wide and 1.05 m high. To simulate limited translational movement of the abutment toe in the physical model test, a beam as a footing was used to support the abutment. The elastic modulus of the zones around the beam was adjusted to approximate abutment toe translation in the physical model test. In addition, the abutment toe was hinged with the footing to allow free abutment rotation. Figure 3.1 shows that the movements of the bottom side, the left side, and the right side of the simulation model in horizontal and vertical directions were restricted.

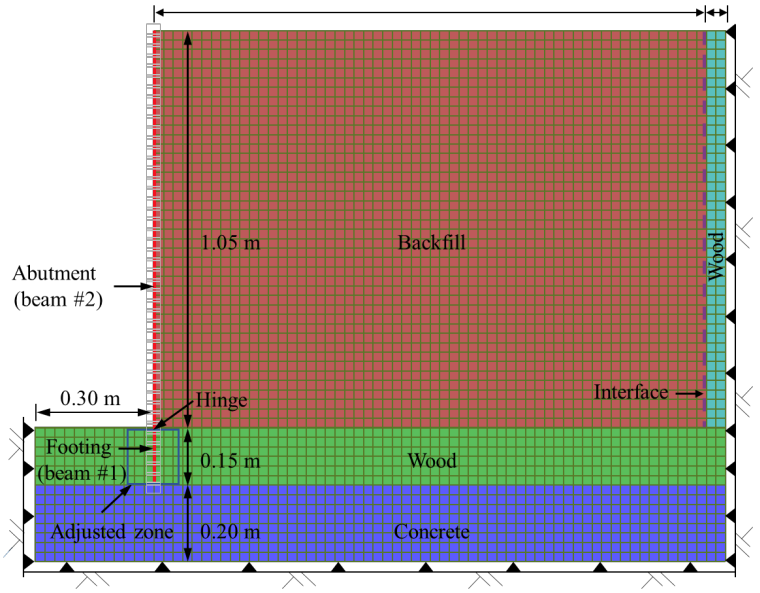

Figure 3.1 Numerical model without mitigation measures (baseline model).

This study utilized the two-dimensional finite difference method-based Fast Lagrangian Analysis of Continua (FLAC2D) software to perform the numerical analysis. The plastic hardening (PH) model in the FLAC2D was used to simulate the behavior of the Kansas River sand and lightweight aggregate backfill. Table 3.1 provides the parameters of the PH model for the sand backfill, which were adopted from Liu et al. (2022d). Low self-weight and high friction angle were the primary material characteristics for lightweight aggregate. Ye et al. (2024) reported that the compacted lightweight aggregate, composed of expanded shale, clay, and slate, had a unit weight of 7.4 kN/m^3 and a peak friction angle of 45° at a relative density of 75%. The lightweight aggregate backfill utilized the same parameters of the PH model as the sand backfill except that the dry density and peak friction angle values were changed to 754 kg/m^3 and 45°, respectively.

Table 3.1 Parameters of plastic hardening model

Properties	Values	Properties	Values
Cohesion, c (kPa)	0	Reference pressure, p_{ref} (kPa)	10
Dry density, ρ (kg/m^3)	1840	Poisson's ratio, μ	0.2
Ultimate dilation angle, ψ_f (degree)	2.0	Failure ratio, R_f	0.90
Secant stiffness, E_{50}^{ref} (MPa)	11.5	Tension limit, σ_t (kPa)	0
Tangent stiffness, E_{oed}^{ref} (MPa)	20.0	Initial void ratio, e_{ini}	0.44
Unloading-reloading Stiffness, E_{ur}^{ref} (MPa)	28.7	Maximum void ratio, e_{max}	0.62
Peak friction angle, φ (°)	40.7	Dimensionless parameter, α	1.75
Elastic modulus exponent, m	0.45	Hardening modulus for cap pressure, H_C (kPa)	1.2×10^4
Overconsolidation ratio, OCR	1		

Table 3.2 lists the parameters of materials in the simulation model while Table 3.3 presents the parameters of the two beams to simulate the footing and the abutment. According to Kulhawy and Mayne (1990), the friction angle of a soil under a plane strain condition is equal to 1.12 times that under a triaxial compression condition. In addition, two reduction factors (R_{int}) of 0.67 and 0.50 were utilized to calculate the interface friction angle and cohesion between the abutment and backfill, and between the backfill and the right wooden plate, respectively, using Equations (1) and (2):

$$\varphi_{int} = \arctan\left(R_{int} \cdot \tan\varphi\right) \tag{1}$$

$$c_{int} = R_{int} c \tag{2}$$

where φ is the friction angle of the backfill and c is the cohesion of the backfill.

The dilation angle for these interfaces was assumed to be 0. According to Itasca (2019), the shear stiffness (k_s) and normal stiffness (k_n) of the interface could be calculated using Equation (3):

$$k_n = k_s = 10 \times \max\left[\frac{(K + 4G/3)}{\Delta_{Z\min}}\right] \quad (3)$$

where K and G are the bulk and shear moduli of neighboring zones, respectively and Δ_{zmin} is the minimum width of the neighboring zone in the normal direction of the interface.

Table 3.2 Parameters of materials in the simulation model

Material	Constitutive model	Parameters
Concrete	Elastic	E=30 GPa, γ =2300 kg/m^3, μ=0.20
Wood	Elastic	E=12.5 GPa, γ =400 kg/m^3, μ=0.40
Adjusted zone	Elastic	E=10 GPa, γ =400 kg/m^3, μ=0.40
Backfill	Plastic hardening	1.12 times peak friction angle and dilation angle of 2°

E = elastic modulus, γ = density, and μ =Poisson's ratio

Table 3.3 Parameters of beams in the simulation model

Beam No.	Representative	Parameters
1	Footing	E=30 GPa, A = 0.06 m^2, I=1.8×10^{-5} m^4
2	Abutment	E=30 GPa, A = 0.12 m^2, I=1.44×10^{-4} m^4

A = cross-section area and I = moment of inertia

The bridge deck was assumed to be integrated with the IBA in spring. The simulation adopted the following steps: (a) construct the base, the footing (beam #1), and the wooden plate, and then run the software until equilibrium is reached; (b) construct the abutment (beam #2) and restrict movement of the abutment at a height of 0.99 m (i.e., abutment top) in the horizontal direction, then run the software until equilibrium is reached; (c) place backfill in equal lifts (50 mm thick per lift), run the software until equilibrium is reached, and continue placing backfill until all lifts are placed (this position is termed as Position I in the first abutment movement cycle, i.e., Position 1-I); (d) move the abutment top 3 mm toward the backfill (Position 1-II) to simulate bridge deck expansion from spring to summer, and then move the abutment top 3 mm away from the backfill (Position 1-III) to simulate bridge deck contraction from summer to fall, followed by another 3-mm movement of the abutment top further away from the backfill (Position 1-IV) to simulate bridge deck contraction from fall to winter. Finally, the abutment top was pushed toward the original position (Position 2-I) to complete the first seasonal temperature change cycle (also start the second seasonal temperature change cycle); (e) repeat Step (d) four times; therefore, five seasonal temperature change cycles are simulated. The speed to move the abutment at the height of 0.99 m was chosen to be 5×10^{-10} m/step to ensure the model was in approximate static equilibrium.

3.2 Numerical model calibration

To calibrate the numerical model, this study compared the computed abutment toe movements, horizontal earth pressures, and backfill surface settlements with those from the model test in Liu et al. (2022c). Figure 3.2 shows the comparisons of the abutment toe movements between the simulation and the physical model test during the five simulated seasonal temperature change cycles. The abutment toe movements shown in Figure 3.2 are relative to the position of the abutment after backfill placement (i.e., Position 1-I). When the abutment top (i.e., at the height of

0.99 m) moved toward the backfill from Position IV to Position II of the next cycle, the abutment toe moved away from the backfill; while the abutment toe moved toward the backfill when the abutment top moved away from the backfill (i.e., from Position II to Position IV). After the first and second seasonal temperature change cycles (i.e., Positions 2-I and 3-I), the abutment toe movements away from the backfill in the simulation matched those in the physical model test. However, the abutment toe had slightly larger movements away from the backfill in the simulation than in the physical model tests after the third, fourth, and fifth seasonal temperature change cycles (i.e., Positions 4-I, 5-I, and 6-I). This movement difference increased with the number of seasonal temperature change cycles. Overall, the abutment toe movements in the simulation matched those in the physical model test.

Figure 3.3 shows the comparison of horizontal earth pressures behind the abutment at Positions 1-I and 1-II in the simulation and the physical model test. At Position 1-I, the horizontal earth pressures at elevations of 0.6 to 1.05 m in the physical model test higher than those in the simulation were caused by residual horizontal stresses from the compaction effects in the physical model test. In general, the horizontal earth pressures at Positions 1-I and 1-II in the simulation are in good agreement with those in the physical model test.

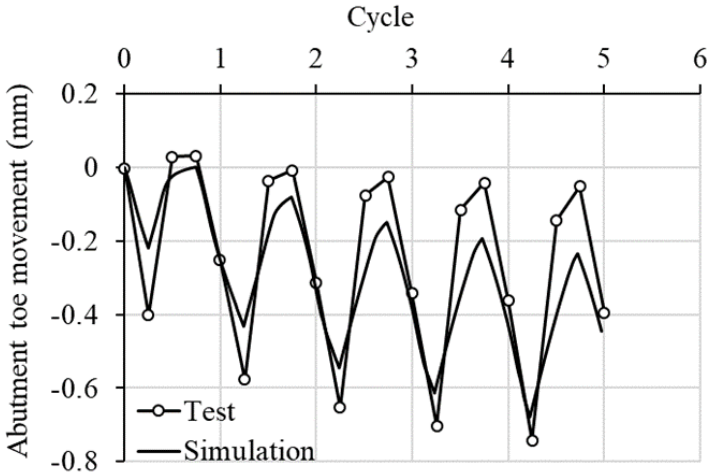

Figure 3.2 Abutment toe movements in the simulation and the physical model test.

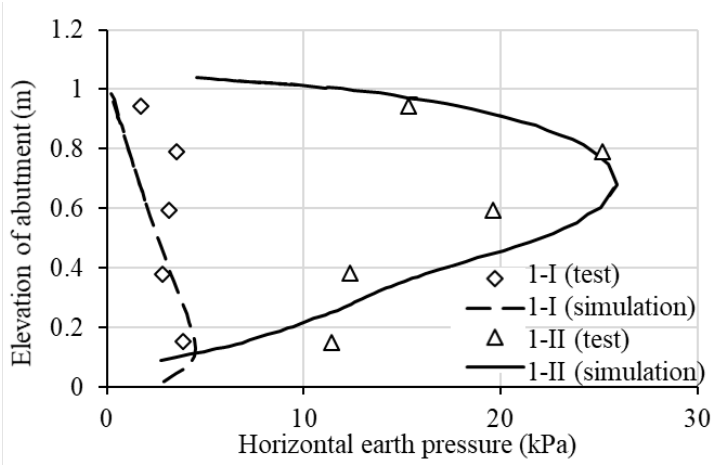

Figure 3.3 Horizontal earth pressures behind the abutment at Positions 1-I and 1-II in the simulation and the physical model test.

Figure 3.4 shows the comparison of backfill surface settlements at distances of 0.05, 0.15, 0.30, and 0.50 m from the back of the abutment between the simulation and the physical model test. As the abutment top moved toward the backfill from Position IV to Position II, the backfill surface in the simulation and the physical model test moved upward; while the backfill surface settled as the abutment top moved away from the backfill from Position II to Position IV. In

addition, the backfill surface settlements at these four distances in the physical model test and the backfill surface settlements at distances of 0.05, 0.15, and 0.30 m in the simulation increased with the number of simulated seasonal temperature change cycles. However, the backfill surface at a distance of 0.50 m in the simulation settled at the beginning and then moved upward (i.e., backfill heave) from the second simulated seasonal temperature change cycle. In general, the physical model test and the simulation model had close magnitudes and variations of backfill surface settlements versus the simulated seasonal temperature change cycles.

The comparisons of the abutment toe movements, horizontal earth pressures, and backfill surface settlements indicate that the numerical model in this study reasonably simulated the behavior of the IBA under seasonal temperature change cycles.

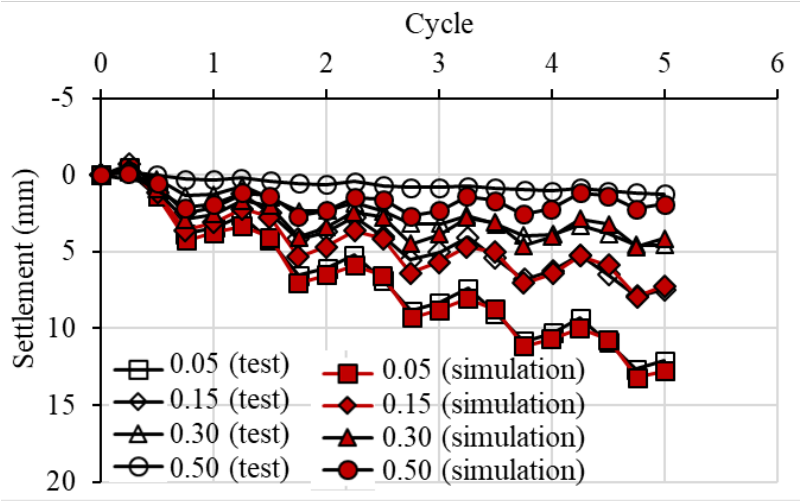

Figure 3.4 Backfill surface settlements at distances of 0.05, 0.15, 0.30 and 0.50 m in the simulation and the physical model test.

3.3 Geosynthetic reinforcement

The strip elements in the FLAC2D were used to simulate the geogrids to reinforce the backfill. Table 3.4 lists the parameters for the strip elements determined from the publication by

Xiao et al. (2016). The elastic modulus at the tensile strain of 1%, the strip tensile yield force limit, and the tensile failure strain limit in Table 3.4 were calculated from the tensile strength tests of a geogrid conducted by Xiao et al. (2016). In addition, the friction coefficient of 0.62 was determined by three pullout tests under normal stresses of 3.5, 7.6, and 11.1 kPa. Figure 3.5 shows the simulation and measured results of the three pullout tests. Figure 3.5 shows that the simulation results using the parameters in Table 3.4 are in good agreement with the test results.

Table 3.4 Parameters of strip elements to simulate geogrid reinforcement

Parameters	Values
Calculation width (m)	1
Elastic modulus (MPa)	457
Initial apparent friction coefficient	0.62
Minimum apparent friction coefficient	0.62
Number of strips per calculation width	1
Shear stiffness (kN/m)	6500
Cohesion (kN/m)	0
Strip thickness (m)	7.6×10^{-4}
Strip width (m)	1
Strip tensile yield force limit (kN)	17.68
Tensile failure strain limit	0.11

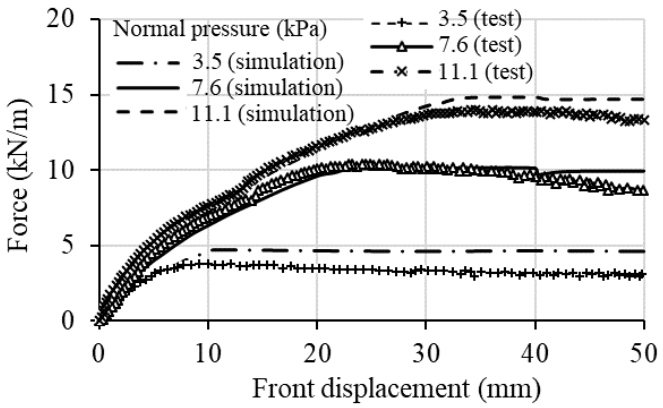

Figure 3.5 Simulation and measured results of geogrid pullout tests.

3.4 Simulation Arrangement

This study performed numerical simulations to investigate the effects of geosynthetic reinforcement and lightweight aggregate on the mitigation of IBA problems induced by seasonal temperature changes. Figure 3.6 shows the simulation arrangement considering the effect of geosynthetic reinforcements. Simulations S1 to S5 all had the sand backfill reinforced by geosynthetics with a vertical spacing of 100 mm. Except for S2 with the geosynthetics connected to the abutment in the front, the front of the geosynthetics in all other simulations was free. The geosynthetics in S1 and S2 were 750 mm long. Simulation S3 had a tier geosynthetic layout, in which the length of the geosynthetic increased from 300 mm at the bottom to 1200 mm at the top (i.e., 100 mm increase per layer). Simulations S4 and S5 had geosynthetic lengths of 500 and 1000 mm, respectively.

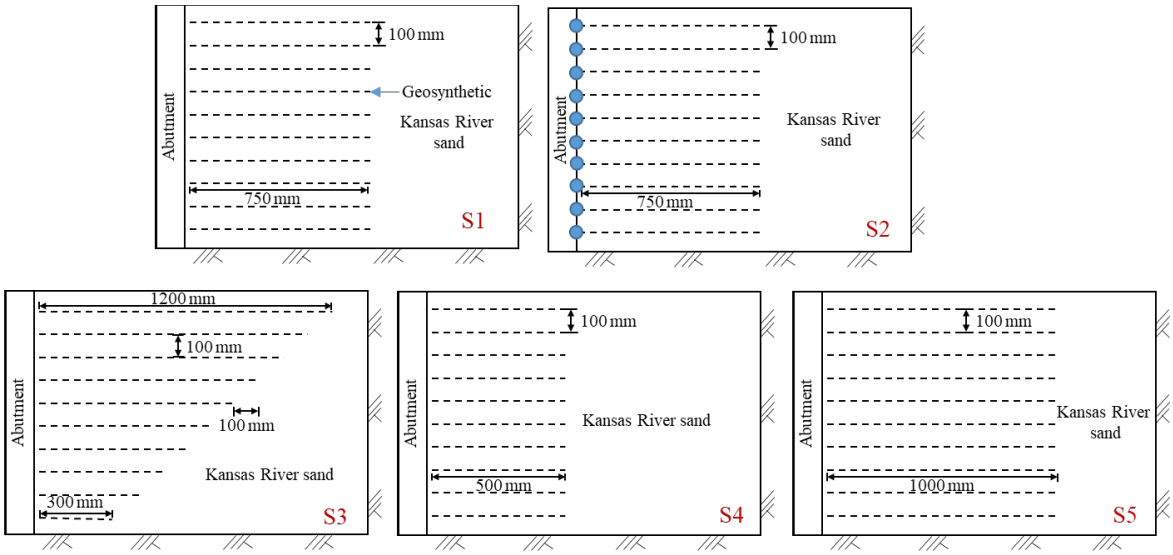

Figure 3.6 Simulation arrangement considering the effect of geosynthetic reinforcement.

Figure 3.7 shows the simulation arrangement considering the effect of lightweight aggregate. The sand backfill in the baseline model was replaced by the lightweight aggregate with a width of 300, 500, 700, and 1450 mm in simulations S6, S7, S8, and S9, respectively. Figure 3.8 shows the simulation arrangement considering the effect of combined measures of lightweight aggregate and geosynthetic reinforcements. Simulations S10, S11, S12, S13, and S14 had the same geosynthetic placement as simulations S1, S2, S3, S4, and S5, respectively, while simulations S10, S11, S12, S13, and S14 all had full lightweight aggregate backfill (i.e., 1450 mm wide).

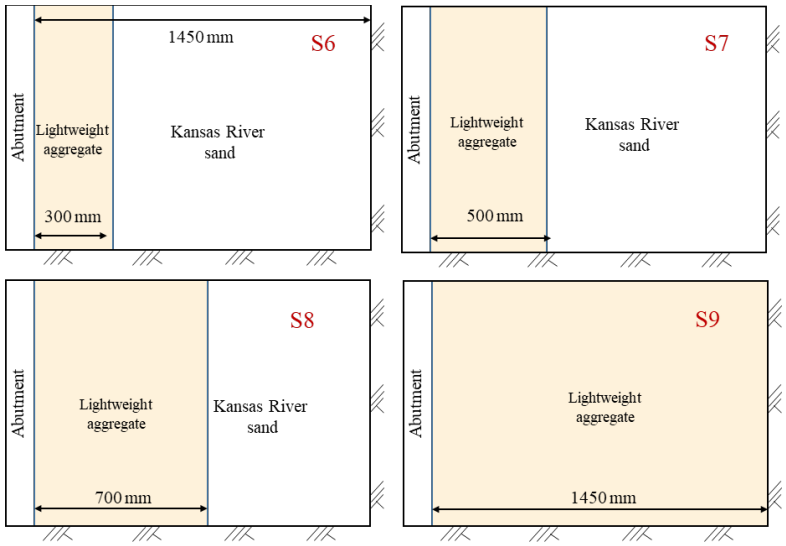

Figure 3.7 Simulation arrangement considering the effect of lightweight aggregate.

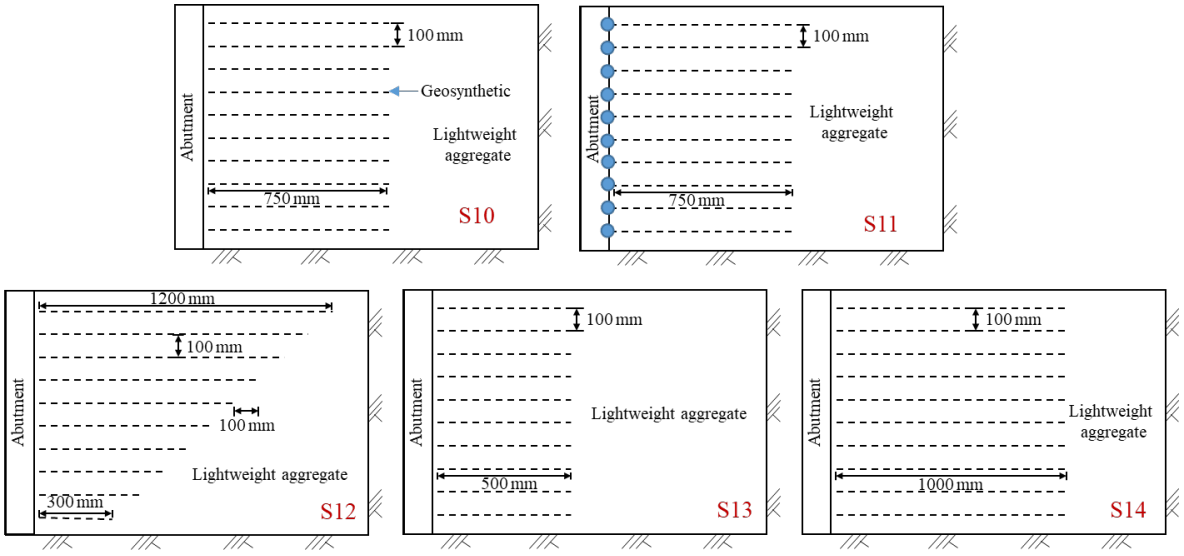

Figure 3.8 Simulation arrangement considering the effect of combined measures of geosynthetic reinforcement and lightweight aggregate.

Chapter 4 Numerical Simulation Results

4.1 Effect of geosynthetic reinforcement

Figure 4.1 shows the effect of geosynthetic reinforcement on the abutment toe movement. As described in the previous subsection, when the abutment top moved toward the backfill from Position IV to Position II, the abutment toe moved away from the backfill; while the abutment toe moved toward the backfill when the abutment top moved away from the backfill (i.e., from Position II to Position IV). Simulations S1, S2, S3, S4, and S5 had less abutment toe movements than the baseline model. The installation of geosynthetic reinforcements slightly reduced the toe movement away from the backfill compared to the baseline model. Simulations S1, S3, S4, and S5 had similar variations of abutment toe movements with the seasonal temperature change cycle. Simulation S2 had smaller abutment toe movements than Simulations S1, S3, S4, and S5, and their difference increased with the seasonal temperature change cycle. The footing restricted the abutment toe movement away from the backfill, while the footing together with the geosynthetic-reinforced backfill within the lower portion restricted the abutment toe movement toward the backfill. Connecting the front of geosynthetics with the bridge abutment further restrained the toe movement.

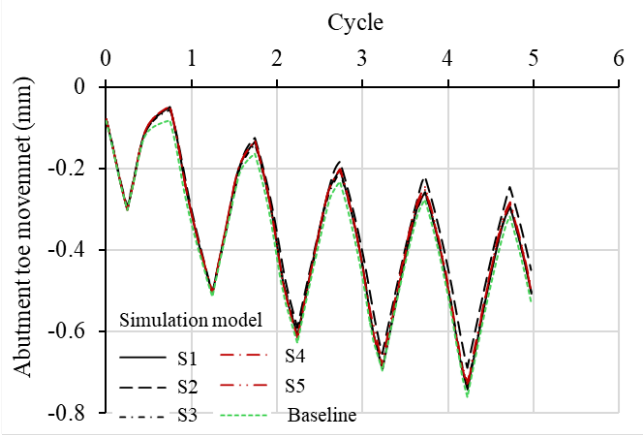

Figure 4.1 Effect of geosynthetic reinforcements on the abutment toe movement.

Figure 4.2 shows the effect of geosynthetic reinforcement on the backfill surface displacement after each cycle, in which the negative surface displacement represents the downward movement of the backfill surface (i.e., backfill settlement) while the positive surface displacement represents the upward movement of the backfill surface (i.e., backfill heave). Figure 4.2 shows that the backfill surface heaved at certain distances after the first or second simulated seasonal temperature change cycle. The backfill heave was partly attributed to the dilatancy of the backfill during continuous shearing. For the simulations with free-front geosynthetic reinforcements (e.g., S1, S3, S4, and S5), horizontal geosynthetics increased the backfill surface settlements right behind the abutment during an early cycle (e.g., Position 1-I) but induced backfill heaves beyond the distance of 0.15 m away from the abutment at a later cycle (e.g., Position 6-I). As the abutment top moved away from the backfill, the geosynthetic-reinforced backfill had a smaller yielding area than the baseline model; therefore, the same abutment top displacement away from the backfill resulted in larger backfill surface settlements right behind the abutment for the geosynthetic-reinforced simulations than those for the baseline model. For the simulations with fixed-front geosynthetic reinforcements (e.g., S2), the geosynthetic reinforcement prevented the front settlement but allowed upward movement behind the abutment. In all cases, the abutment had the same top movement resulting from bridge expansion or contraction, which required a similar volume change (different toe movements might slightly affect the amount of volume change in different cases). Since the backfill right behind the abutment in Simulation S2 could not settle due to the reinforcement connection to the abutment and the backfill at the distance of 0.6 to 1.45 m away from the abutment settled, the settled backfill resisted the push-back movement, resulting the backfill heave within the distance of 0 to 0.6 m behind the abutment.

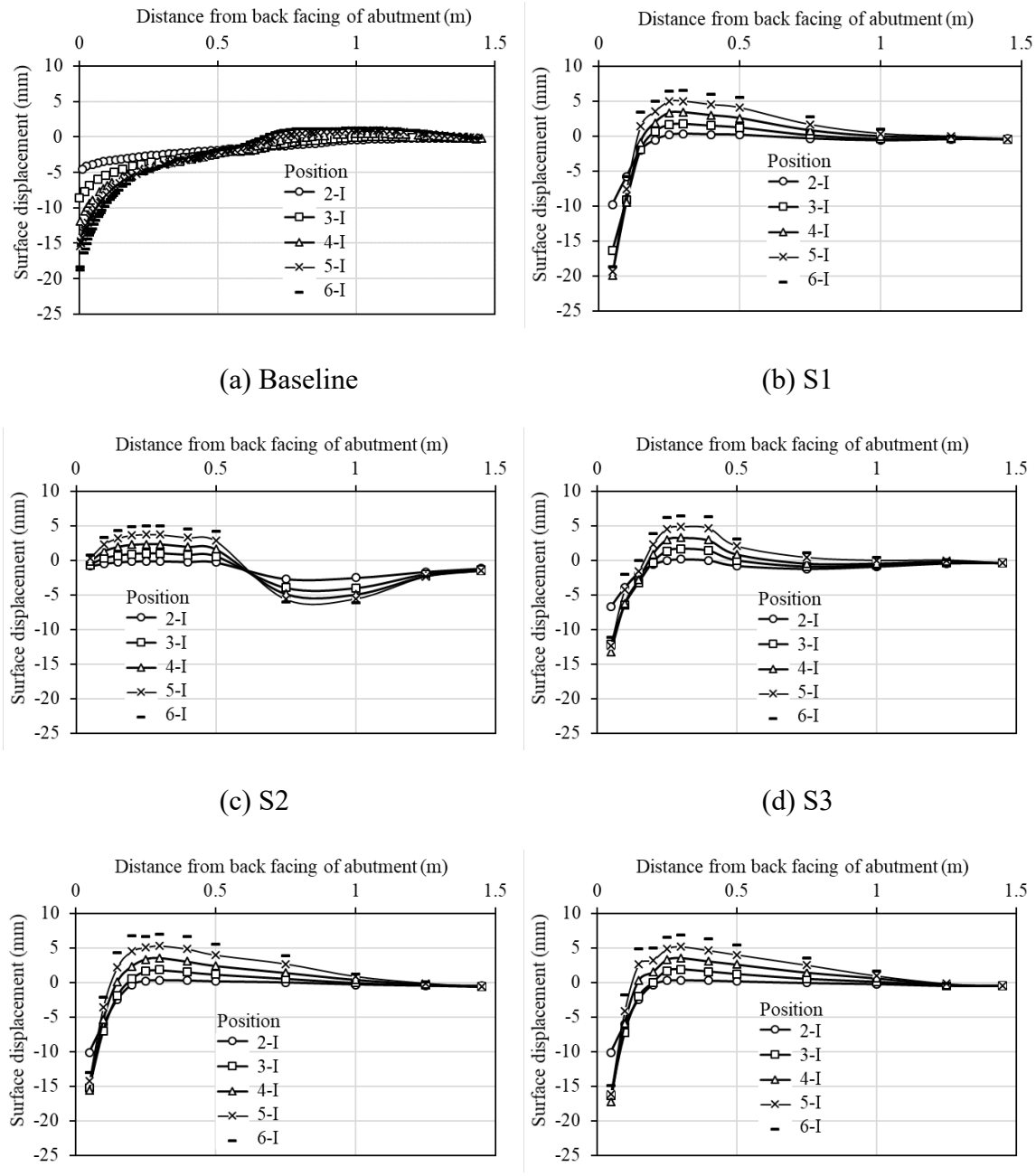

Figure 4.2 Effect of geosynthetic reinforcement on the backfill surface displacements after each cycle.

Figure 4.3 shows the effects of geosynthetic reinforcement on the shear strain increments in the backfill at Position 6-I (the abutment top returning to the original position) after five cycles.

The baseline model had both potential active and passive shear slip surfaces. The active shear slip surfaces occurred when the bridge abutment top moved away from the backfill and the passive shear slip surfaces occurred when the bridge abutment top moved toward the backfill. For simulations with free-front geosynthetic reinforcements (e.g., S1, S3, S4, and S5), the geosynthetic reinforcement minimized the development of active and passive shear slip surfaces but increased the shear strain increments right behind the bridge abutment. For simulations with fixed-front geosynthetic reinforcements (e.g., S2), the geosynthetic reinforcements reduced the shear strain increments right behind the bridge abutment but increased the shear strain increments at the back end of the geosynthetic reinforcements (i.e., at the distance of 0.75 m from the bridge abutment) and formed a vertical shear band. These phenomena indicate a composite mass was formed behind the abutment. In addition, Simulation S2 had shear strain increments at the geosynthetic-soil interface at elevations of 0.6 to 1.05 m, indicating potential reinforcement pullout within the upper backfill.

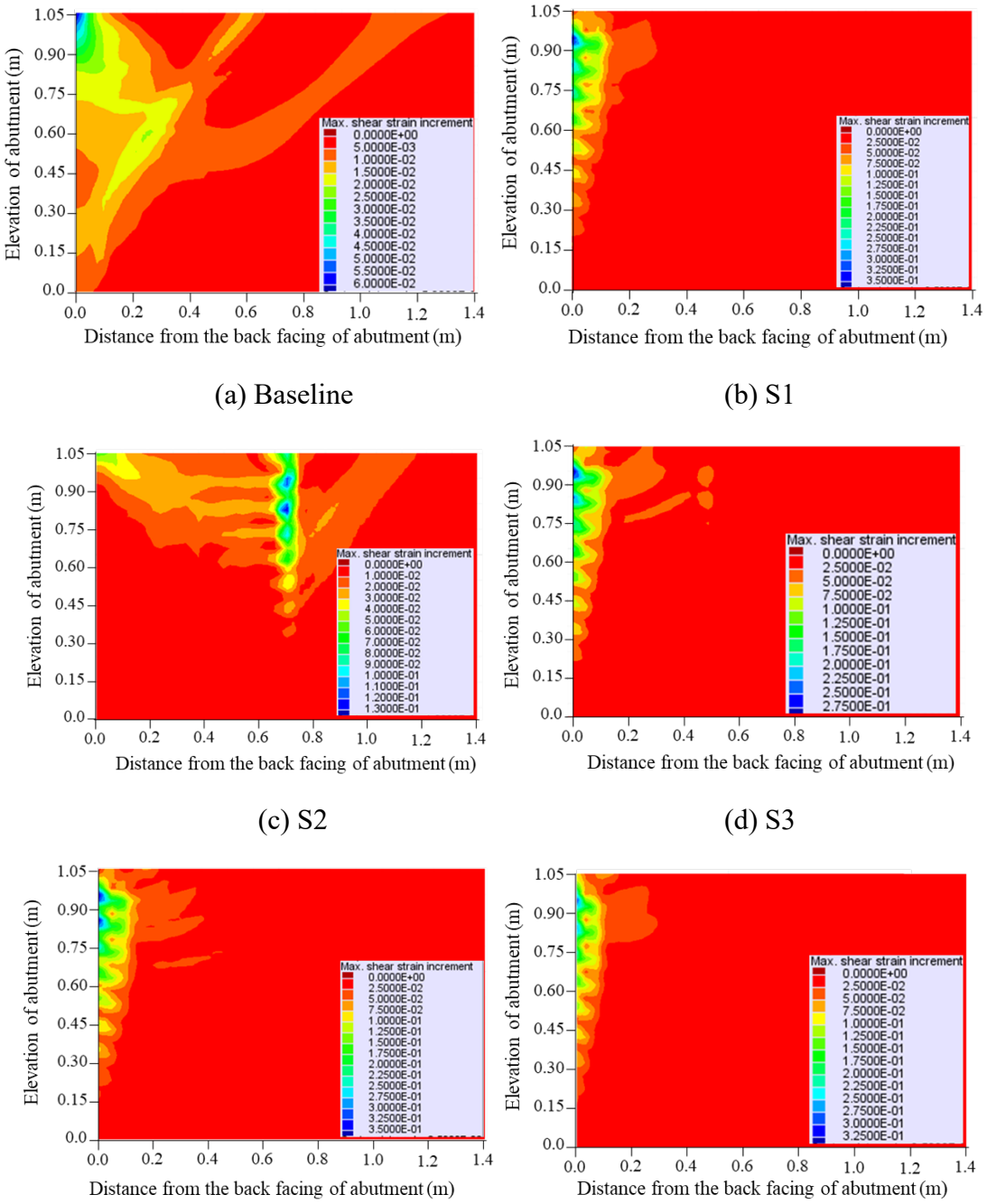

Figure 4.3 Shear strain increments in the backfill after five cycles for (a) baseline model, (b) S1, (c) S2, (d) S3, (e) S4, and (f) S5.

Figure 4.4 shows the effects of geosynthetic reinforcement on the horizontal earth pressures behind the abutment at Positions 1-I and 1-II. The figure includes Jaky's at-rest and Rankine's active and passive pressures for comparison. The plane strain peak friction angle (i.e., 45.6° = 1.12×40.7°) of the sand was used to calculate the horizontal earth pressures. The computed horizontal earth pressures behind the abutment at these positions increased with the decrease of elevation to the maximum value and then decreased with the continued decrease of elevation. The maximum horizontal earth pressure at Position 1-II was located at a higher elevation than that at Position 1-I. Simulations S1, S3, S4, and S5 had similar variations and magnitudes of horizontal earth pressures with elevation of the abutment at Position 1-I. Simulation S2 and the baseline model had similar variations and magnitudes of horizontal earth pressures with elevation of the abutment at Position 1-I. Simulation S2 and the baseline model had higher maximum horizontal earth pressures than Simulations S1, S3, S4, and S5 at Position 1-I. The front connection of geogrids to the abutment reduced the horizontal earth pressures within the lower portion of the abutment but increased those within the upper portion. Simulations S1, S2, S3, S4, S5, and the baseline model had similar variations and magnitudes of horizontal earth pressures versus the abutment elevation at Position 1-II. The geosynthetic reinforcement did not have any obvious effects on the horizontal earth pressures behind the abutment at Position 1-II because the reinforcement was under compression. Geosynthetic reinforcement is effective only under tension. The computed horizontal earth pressures at Position 1-I were close to Jaky's at-rest pressures but higher than Rankine's active pressures above the elevation of 0.1 m, while the computed horizontal earth pressures at Position 1-II were higher than Jaky's at-rest pressures above the elevation of 0.1 m but lower than Rankine's passive pressures below the elevation of 0.8 m. In addition, the computed horizontal pressures above the elevation of 0.8 m were higher than Rankine's passive

pressures when the abutment was at Position 1-II. The reason for the computed horizontal pressures lower than Rankine's active pressure or higher than Rankine's passive pressure is because Rankine's theory assumed no interface friction between abutment and backfill instead of actual interface friction.

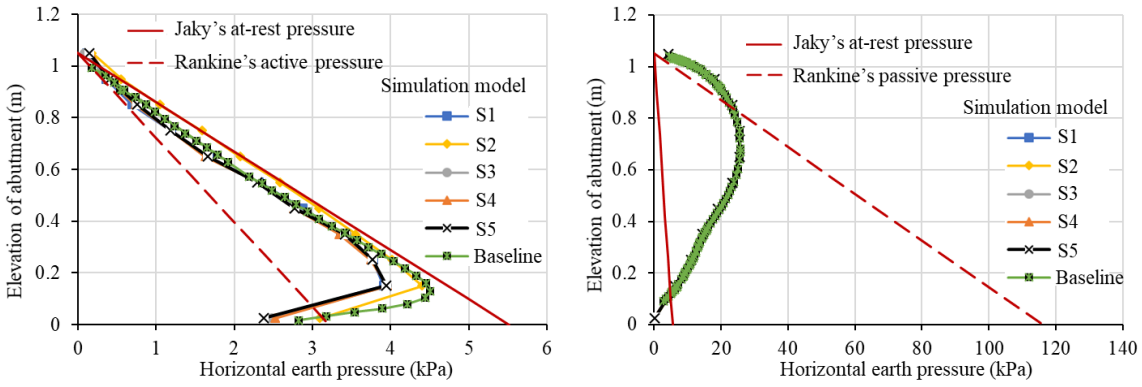

(a) (b)

Figure 4.4 Effect of geosynthetic reinforcement on horizontal earth pressures behind the abutment at (a) Position 1-I and (b) Position 1-II.

4.2 Effect of lightweight aggregate

Figure 4.5 shows the effect of lightweight aggregate on the abutment toe movement. Simulations S6, S7, S8, and S9 had less abutment toe movements than the baseline model. The use of lightweight aggregate reduced the abutment toe movement. More replacement of the sand with the lightweight aggregate resulted in less abutment toe movements. The lightweight aggregate backfill had lower horizontal earth pressures on the abutment due to low self-weight, thereby reducing the abutment toe movement during the cycle.

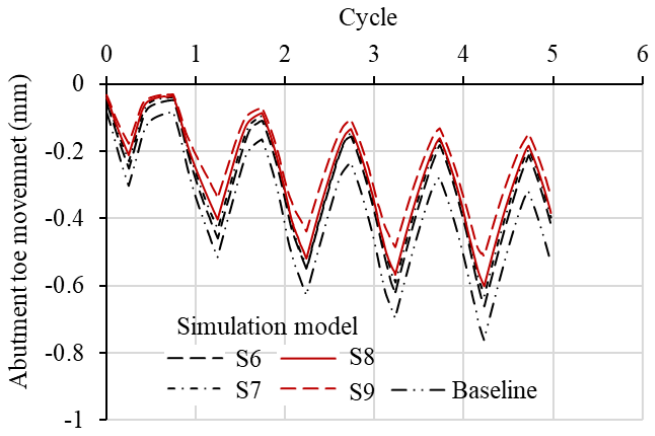

Figure 4.5 Effect of the lightweight aggregate on the abutment toe movement.

Figure 4.6 shows the effect of lightweight aggregate on backfill surface displacement after each cycle. For simulation S6 with a lightweight aggregate zone of 0.3 m wide, the backfill surface heaved at distances of 0.1 to 0.3 m away from the abutment, beyond which the backfill surface settled and its settlement decreased as the distance from the abutment increased. For simulation S7 with the lightweight aggregate zone of 0.5 m wide, the backfill surface settled right behind the abutment and its settlement decreased with distance. This was followed by heaving within a short distance until 0.45 m, beyond which the backfill surface settled, again decreasing with distance. For simulations S8 and S9 with the lightweight aggregate zone of 0.7 and 1.45 m wide, respectively, the backfill surface settled at distances of 0 to 0.5 m, beyond which the backfill surface slightly settled during an early cycle (e.g., Positing 1-I) but heaved at a later cycle (e.g., Positing 6-I). In general, the increase of the lightweight aggregate zone width increased the surface settlement right behind the bridge abutment but reduced the displacement at the interface between the lightweight aggregate and the sand. Both backfill settlement and heave in simulations S6 to S9 increased with the cycle, indicating that the temperature change increased differential settlement.

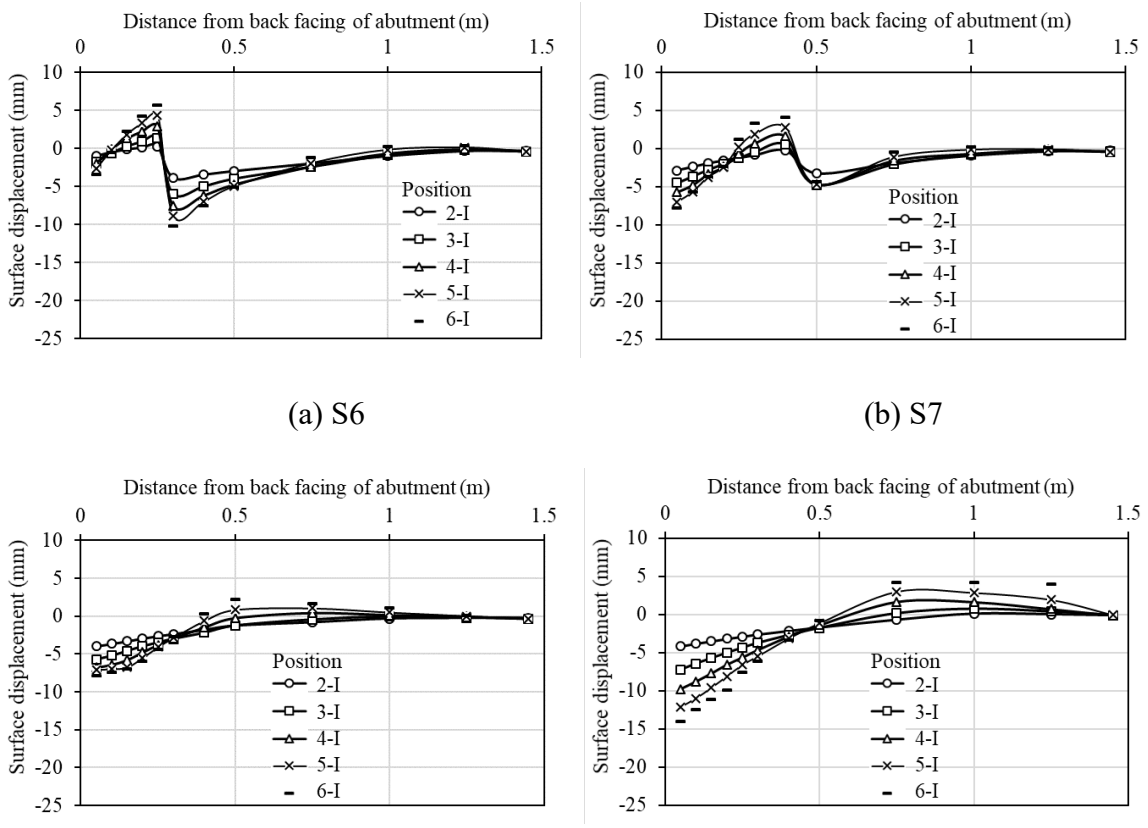

Figure 4.6 Effect of the lightweight aggregate zone width on the backfill surface displacements.

Figure 4.7 shows the effect of the lightweight aggregate on the shear strain increment in the backfill at Position 6-I after five cycles. The simulations with the lightweight aggregate showed multiple potential active and passive shear slip surfaces. With the increase of the lightweight aggregate zone width, the passive shear slip surfaces were more concentrated and obvious. The normal stress and backfill friction angle have significant effects on the shear strength. Since the lightweight aggregate had a lower density (i.e., approximately one-third that of the sand), the aggregate had lower self-weight and shear strength, resulting in more shear slip surfaces under continuous shearing.

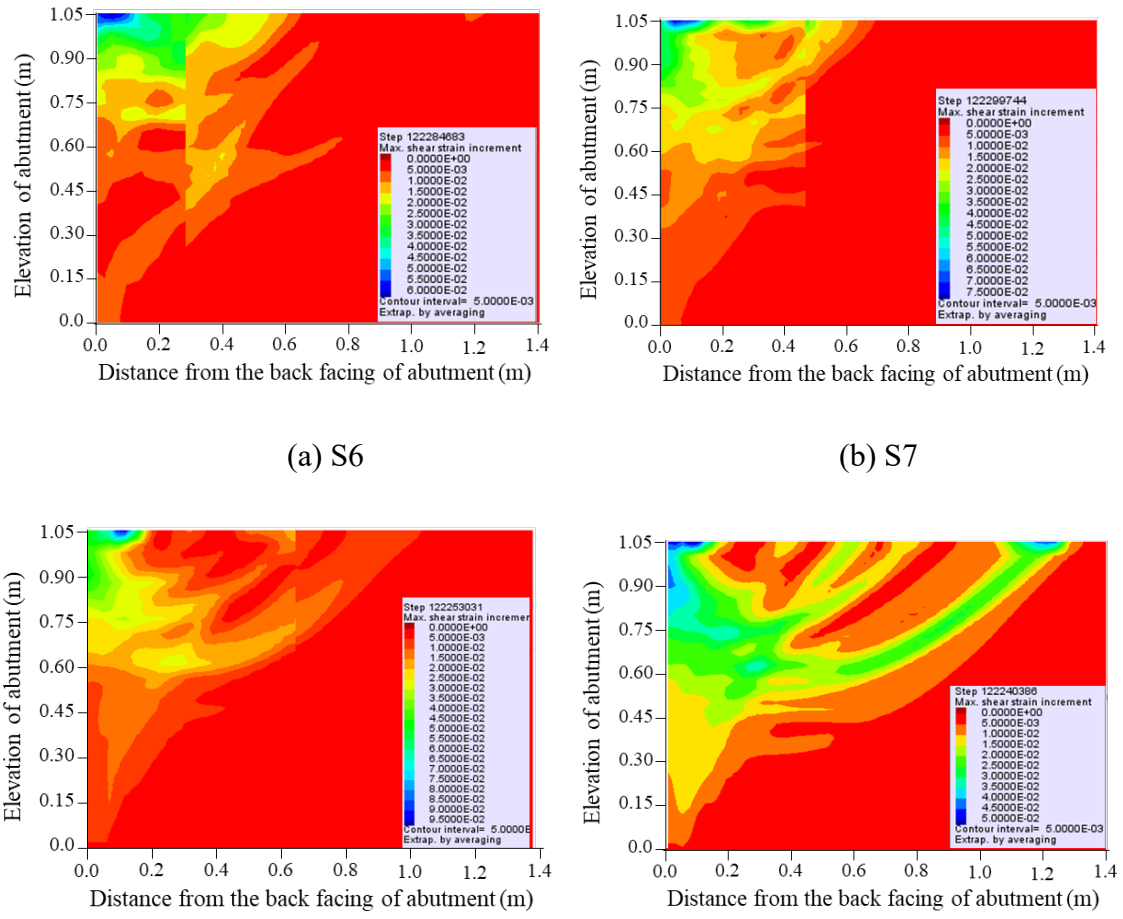

(a) S6 (b) S7

(c) S8 (d) S9

Figure 4.7 Effect of the lightweight aggregate zone width on the shear strain increment.

Figure 4.8 shows the effect of the lightweight aggregate zone width on the horizontal earth pressure behind the abutment at Positions 1-I and 1-II by comparing Jaky's at-rest and Rankine's active and passive pressures. The plane strain peak friction angle (i.e., 50.4° = 1.12×45°) of the lightweight aggregate was used to calculate horizontal earth pressures. The lightweight aggregate reduced the horizontal earth pressures behind the abutment at Positions 1-I and 1-II compared to the baseline model. Replacing more sand with the lightweight aggregate resulted in a greater reduction of horizontal earth pressures. The computed horizontal earth pressures at Position 1-I in

simulation S9 were close to Jaky's at-rest pressures, while the computed horizontal earth pressures at Position 1-I in simulations S6, S7, and S8 were higher than Jaky's at-rest and Rankine's active pressures above the elevation of 0.1 m. The computed horizontal earth pressures at Position 1-II were higher than Jaky's at-rest pressures above the elevation of 0.1 m, but lower than Rankine's passive pressures below the elevation of 0.6 to 0.8 m. The computed horizontal pressures at this elevation were higher than Rankine's passive pressures at Position 1-II.

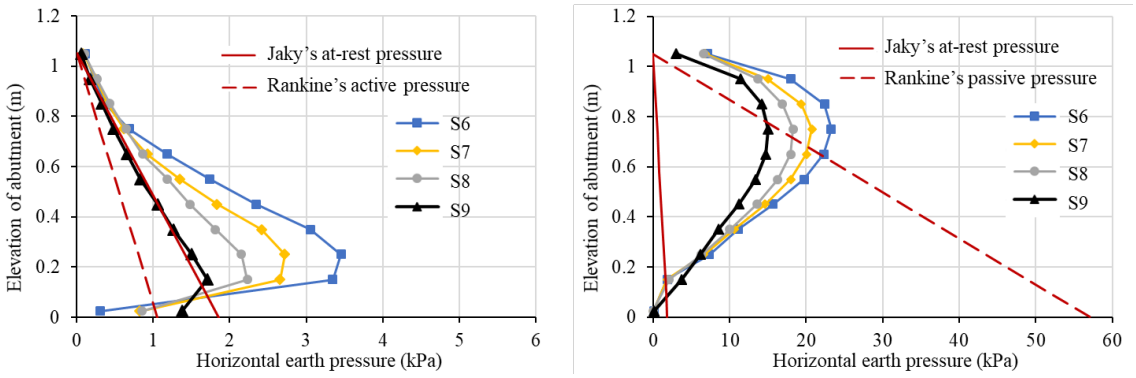

Figure 4.8 Effect of the lightweight aggregate zone width on horizontal earth pressures behind the abutment at (a) Position 1-I and (b) Position 1-II.

4.3 Combined effect of lightweight aggregate and geosynthetic reinforcement

Figure 4.9 shows the combined effect of the lightweight aggregate and the geosynthetic reinforcements on the abutment toe movement. Simulations S10, S12, S13, and S14 had similar variations and magnitudes of the abutment toe movement with the temperature change cycle, while simulation S11 had smaller abutment toe movements than simulations S10, S12, S13, and S14 due to the constraints of the geosynthetic reinforcements connected to the abutment. The abutment with the geosynthetic-reinforced lightweight aggregate had smaller abutment toe movements than that with unreinforced and geosynthetic-reinforced sand. The combined measures of geosynthetic

reinforcements and lightweight aggregate effectively reduced the abutment toe movement.

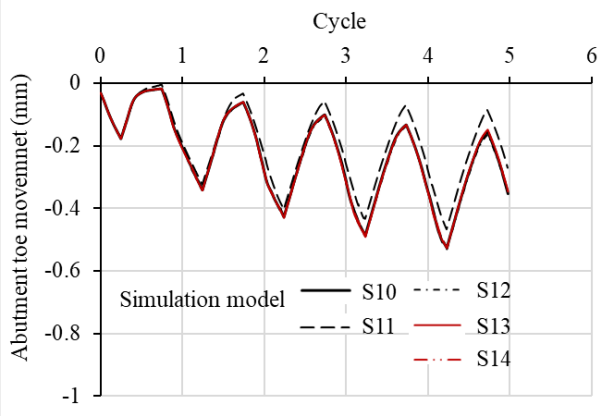

Figure 4.9 Effect of lightweight aggregate and geosynthetic reinforcements on the abutment toe movement.

Figure 4.10 shows the combined effect of the lightweight aggregate and the geosynthetic reinforcements on the backfill surface displacement after each cycle. For the simulations with geosynthetic reinforcements free at the front (e.g., S10, S12, S13, and S14), the backfill surface settled within 0.15 m from the back of the abutment, beyond which the backfill surface heaved. In the simulations with geosynthetic reinforcements connected to the abutment (e.g., S11), the backfill surface heaved within the distance of 0.5 m from the back of the abutment, beyond which the backfill surface settled at the distance of 1 to 1.45 m from the back of the abutment. Clearly, this case had the least differential settlement between the abutment and the backfill so that the bump was minimized. The backfill surface in simulations of the abutment with the geosynthetic-reinforced lightweight aggregate settled less behind the abutment than that with the unreinforced and geosynthetic-reinforced sand at the same temperature change cycle.

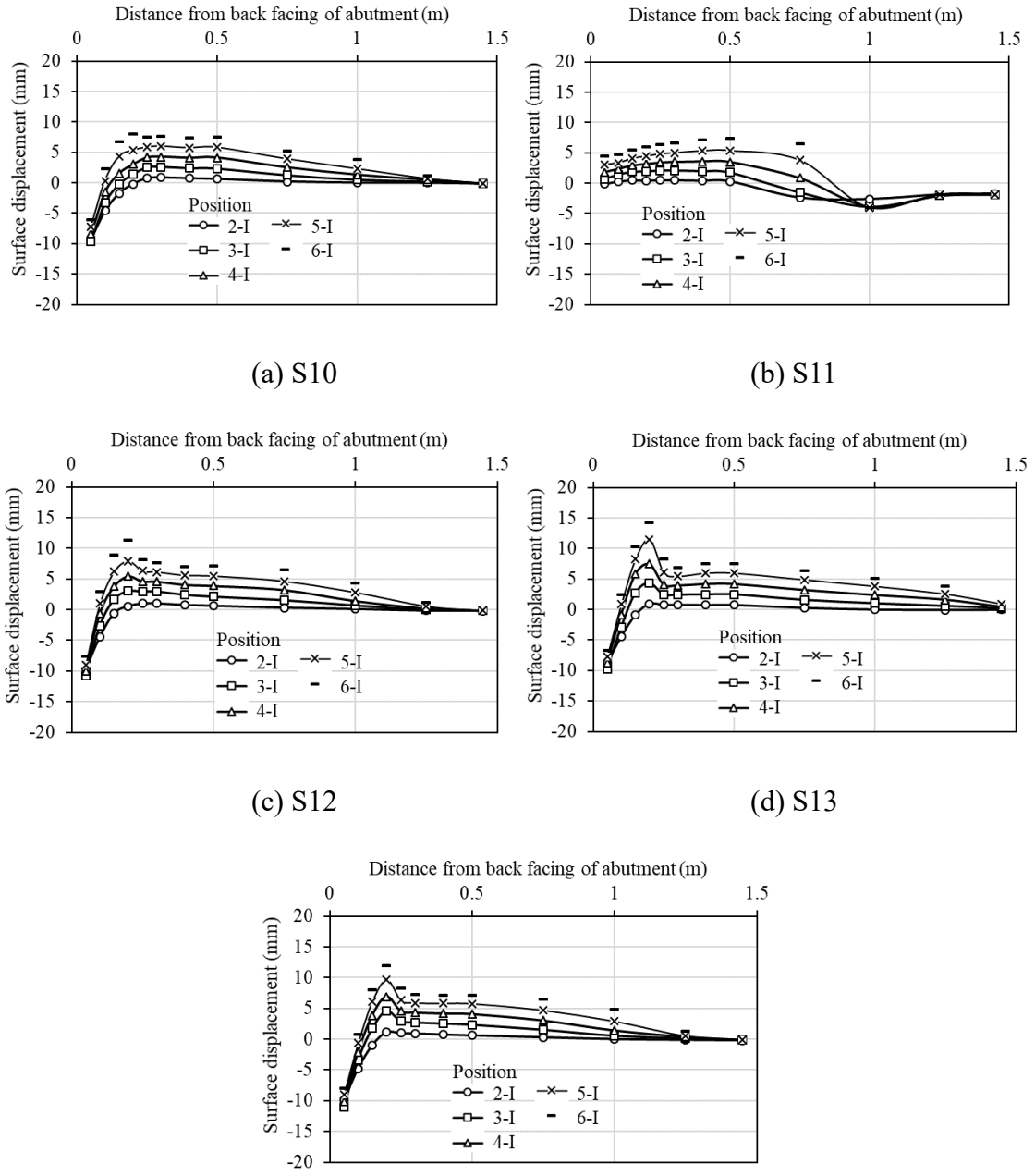

Figure 4.10 Effect of the lightweight aggregate and the geogrid reinforcements on the backfill surface displacement.

Figure 4.11 shows the combined effect of the lightweight aggregate and the geosynthetic reinforcement on the shear strain increment in the backfill at Position 6-I after five cycles. As

mentioned in the previous subsection, the geosynthetic reinforcement minimized the development of shear failure surfaces but increased the shear strain increment right behind the abutment. Simulations S10, S11, S12, S13, and S14 had similar shear strain distributions to simulations S1, S2, S3, S4, and S5, respectively. The geosynthetics connected to the abutment backfilled with the lightweight aggregate (simulation S11) had more obvious pullout potential than those backfilled with the sand (simulation S2) because the lightweight aggregate generated low overburden pressures due to low self-weight so that the geosynthetic reinforcement at the same elevation had lower pullout resistance in the lightweight aggregate than in the sand.

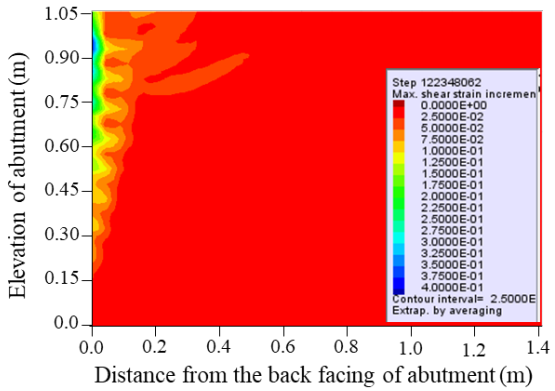

(a) S10

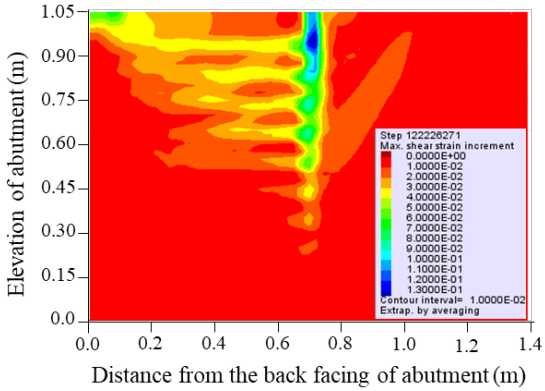

(b) S11

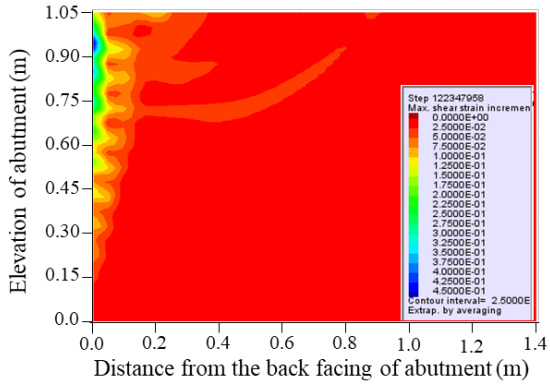

(c) S12

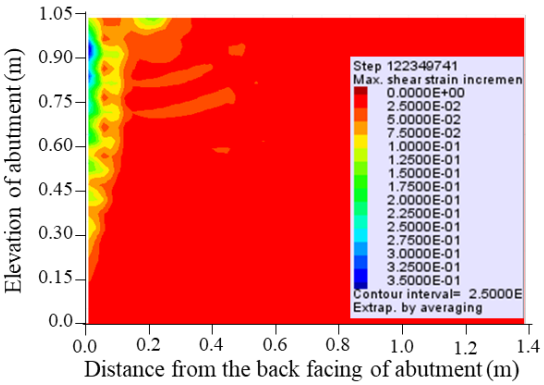

(d) S13

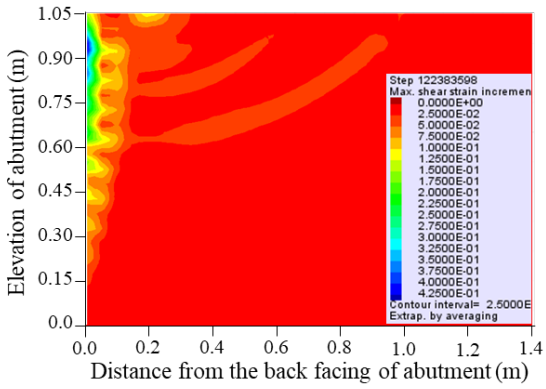

(e) S14

Figure 4.11 Effect of the lightweight aggregate and the geosynthetic reinforcements on the shear strain increment (continued).

Figure 4.12 shows the combined effect of the lightweight aggregate and the geosynthetic reinforcement on the horizontal earth pressure behind the abutment at Positions 1-I and 1-II. The figure includes Jaky's at-rest and Rankine's active and passive pressures based on the plane strain peak friction angle of the lightweight aggregate. Simulations S10, S11, S12, S13, and S14 had lower horizontal earth pressures than the baseline model at Positions 1-I and 1-II. The geogrid reinforcement did not have significant effects on the horizontal earth pressure behind the abutment at Positions 1-I and 1-II except for the case where the geosynthetics connected to the abutment increased the horizontal earth pressure at Position 1-I compared to when there was no geosynthetic connection at the front. The computed horizontal earth pressures at Position 1-I were close to Jaky's at-rest pressures but higher than Rankine's active pressures. The computed horizontal earth pressures at Position 1-II were higher than Jaky's at-rest pressures above the elevation of 0.1 m, but lower than the Rankine's passive pressures below the elevation of 0.8 m.

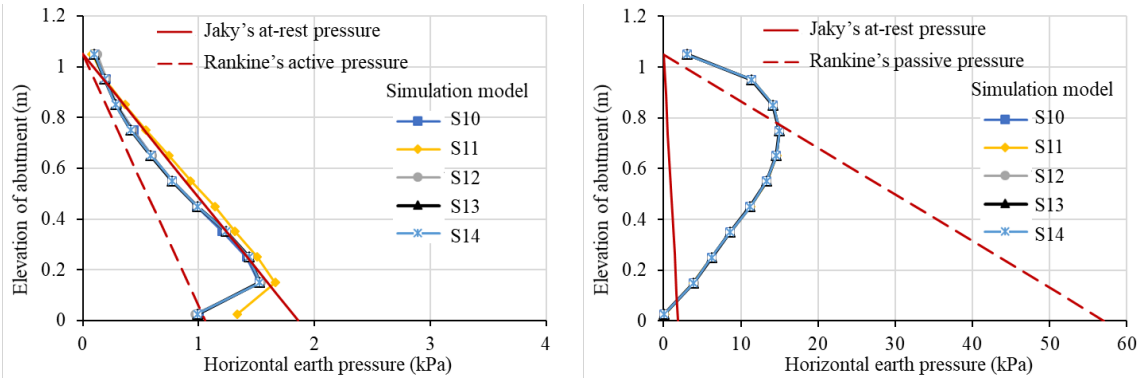

(a) (b)

Figure 4.12 Effects of the lightweight aggregate and the geosynthetic reinforcement on horizontal earth pressures behind the abutment at (a) Position 1-I and (b) Position 1-II.

Chapter 5 Conclusions

This numerical study evaluated the effects of lightweight aggregate and geosynthetic reinforcement on the behavior of IAB subjected to simulated temperature change cycles. In each simulation, the bridge deck was assumed to be integrated with the abutment in spring (i.e., Position 1-I). Bridge deck expansion due to temperature increase from spring to summer pushed the abutment toward the backfill (i.e., Position 1-II), and then bridge deck contraction due to temperature decrease from summer to fall pulled the abutment away from the backfill (i.e., Position 1-III), followed by additional abutment movement away from the backfill in winter (i.e., Position 1-IV). Each numerical model simulated five seasonal temperature change cycles. Based on the numerical results, the following conclusions can be made:

(1) Geosynthetic reinforcement without any connection to the abutment increased the settlement of the backfill right behind the abutment and reduced the settlement of the backfill away from the abutment. However, geosynthetic reinforcements connected to the abutment reduced the settlement of the reinforced backfill and increased the settlement of the unreinforced backfill behind the reinforced zone. Overall, geosynthetic reinforcement connected to the abutment reduced the differential settlement behind the abutment so that the bump at the end of the bridge was minimized.

(2) The lightweight aggregate reduced the horizontal earth pressure behind the abutment. In addition, the lightweight aggregate reduced the abutment toe movement but might form multiple active and passive shear slip surfaces after cycles.

(3) The combined measures of the lightweight aggregate and the geosynthetic reinforcements connected to the abutment effectively reduced the differential settlement behind the abutment, minimized the potential of forming active and passive shear slip surfaces within the backfill, and reduced the horizontal earth pressures behind the abutment.

References

Alqarawi, A., Leo, C., Liyanapathirana, D., & Ekanayake, S. (2016). A study on the effects of abutment cyclic movements on the approach of integral abutment bridges. *Australian Geomechanics*, 51(2), 1-3.

Al-Qarawi, A., Leo, C., & Liyanapathirana, D. S. (2020). Effects of wall movements on performance of integral abutment bridges. *International Journal of Geomechanics*, *20*(2), 04019157.

Abdullah, A., & El Naggar, H. (2023). Soil-structure interaction of integral abutments. *Transportation Geotechnics*, 38, 100900.

Burke, M. P. (1993). Design of integral concrete bridges. *Concrete International*, 15(6), 37-42.

Caristo, A., Barnes, J., & Mitoulis, S. A. (2018, September). Numerical modelling of integral abutment bridges under seasonal thermal cycles. In Proceedings of the Institution of Civil Engineers-Bridge Engineering (Vol. 171, No. 3, pp. 179-190). Thomas Telford Ltd.

Cui, L., & Mitoulis, S. (2015). DEM analysis of green rubberised backfills towards future smart integral abutment bridges (IABs). Geomechanics from Micro to Macro. I, II, 583-588.

Duda, A., & Siwowski, T. (2020). Pressure evaluation of bridge abutment backfill made of waste tyre bales and shreds: experimental and numerical study. *Transportation Geotechnics*, 24, 100366.

Farhangi, V., Zadehmohamad, M., Monshizadegan, A., Izadifar, M., Moradi, M. J., & Dabiri, H. (2023). Effects of geogrid reinforcement on the backfill of integral bridge abutments. *Buildings*, 13(4), 853.

Hoppe, E. J. (2005). Field study of integral backwall with elastic inclusion (No. FHWA/VTRC 05-R28). Virginia Transportation Research Council (VTRC).

Itasca (2019). User's guide for FLAC2D Version 8.0. Itasca Consulting Group, Minneapolis, Minnesota, USA

Khodair, Y., & Hassiotis, S. (2013). Numerical and experimental analyses of an integral bridge. *International Journal of Advanced Structural Engineering*, 5, 1-12.

Kulhawy, F.H., Mayne, P.W., (1990). Manual on estimating soil properties for foundation design. Technical Report No. EPRI-EL-6800.

Liu, H., Han, J., & Parsons, R. L. (2021). Mitigation of seasonal temperature change-induced problems with integral bridge abutments using EPS foam and geogrid. *Geotextiles and Geomembranes*, 49(5), 1380-1392.

Liu, H., Han, J., & Parsons, R. L. (2022a). Integral bridge abutments in response to seasonal temperature changes: state of knowledge and recent advances. *Frontiers in Built Environment*,

8, 916782.

Liu, H., Han, J., & Parsons, R. L. (2022b). Settlement and horizontal earth pressure behind model integral bridge abutment induced by simulated seasonal temperature change. Journal of Geotechnical and Geoenvironmental Engineering, 148(6), 04022043.

Liu, H., Parsons, R. L., Han, J., Ye, Y., & O'Reilly, M. (2022c). Field Pullout Tests of Steel Strips in Lightweight Cellular Concrete Backfill. *Journal of Geotechnical and Geoenvironmental Engineering*, 148(5), 06022004.

Liu, H., Han, J., & Parsons, R. L. (2022d). Effects of seasonal temperature change-induced abutment movements on backfill surface settlements behind integral bridge abutments–Numerical analysis. *Computers and Geotechnics*, 149, 104884.

Liu, H., Han, J., & Parsons, R. L. (2023). Numerical analysis of geosynthetics to mitigate seasonal temperature change-induced problems for integral bridge abutment. *Acta Geotechnica*, 18(2), 673-693.

Liu, G., LaFave, J. M., & Fahnestock, L. A. (2025). Parametric Assessment of Structural Behavior of Integral Abutment Bridge Approach Slabs When Subjected to Live Load and Thermal Effects. *Journal of Bridge Engineering*, 30(6), 04025032.

Zadehmohamad, M., & Bazaz, J. B. (2019). Cyclic behaviour of geocell-reinforced backfill behind integral bridge abutment. *International Journal of Geotechnical Engineering*, 13(5), 438-450.

Oesterle, R.G., Tabatabai, H., Lawson, T.J., Refai, T.M., Volz, J.S. and Scanlon, A. (1998) Jointless and Integral Abutment Bridges Summary Report, (CTL: Skokie, IL, to be published, under review by FHWA).

Puppala, A. J., Saride, S., Yenigalla, R. V., Chittoori, B. C., & Archeewa, E. (2017). Long-term performance of a highway embankment built with lightweight aggregates. *Journal of Performance of Constructed Facilities*, 31(5), 04017042.

Saride, S., Puppala, A. J., Williammee, R., & Sirigiripet, S. K. (2010). Use of lightweight ECS as a fill material to control approach embankment settlements. *Journal of Materials in Civil Engineering*, *22*(6), 607-617.

Tatsuoka, F., Hirakawa, D., Nojiri, M., Aizawa, H., Nishikiori, H., Soma, R., & Watanabe, K. (2009). A new type of integral bridge comprising geosynthetic-reinforced soil walls. *Geosynthetics International*, 16(4), 301-326.

Xiao, C., Han, J., & Zhang, Z. (2016). Experimental study on performance of geosynthetic-reinforced soil model walls on rigid foundations subjected to static footing loading. *Geotextiles and geomembranes*, 44(1), 81-94.

Ye, Y., Han, J., Liu, H., Rachford, S. M., Parsons, R. L., Dolton, B., & O'Reilly, M. (2022). Pullout resistance of geogrid and steel reinforcement embedded in lightweight cellular concrete backfill. *Geotextiles and Geomembranes*, 50(3), 432-443.

Ye, Y. Q., Han, J., O'Reilly, M., Dolton, B., & Parsons, R. L. (2024). Experimental study on physical and mechanical properties of lightweight cellular concrete specimens cast in field and laboratory. *Transportation Research Record*, 2678(10), 67-84.

Yu, W., Liang, X., Ni, F. M. W., Oyeyi, A. G., & Tighe, S. (2020). Characteristics of lightweight cellular concrete and effects on mechanical properties. *Materials*, 13(12), 2678.

Zadehmohamad, M., & Bazaz, J. B. (2019). Cyclic behaviour of geocell-reinforced backfill behind integral bridge abutment. *International Journal of Geotechnical Engineering*, 13(5), 438–450.

Zadehmohamad, M., Bazaz, J. B., Riahipour, R., & Farhangi, V. (2021). Physical modeling of the long-term behavior of integral abutment bridge backfill reinforced with tire-rubber. *International Journal of Geo-Engineering*, 12, 1-19.